ULTRASONIC IMAGING 12, 58-70, (1990)

BACKSCATTER COEFFICIENT MEASUREMENTS USING A REFERENCE PHANTOM TO EXTRACT DEPTH-DEPENDENT INSTRUMENTATION FACTORS

Lin Xin Yao[1], James A. Zagzebski[1,2] and Ernest L. Madsen[1]

Department of Medical Physics[1], Radiology[2] and Human Oncology[2]
1530 Medical Science Center
University of Wisconsin-Madison
Madison WI 53706

In previous work, we demonstrated that accurate backscatter coefficient measurements are obtained with a data reduction method that explicitly accounts for experimental factors involved in recording echo data. An alternative, relative processing method for determining the backscatter coefficient and the attenuation coefficient is presented here. This method involves comparison of echo data from a sample with data recorded from a reference phantom whose backscatter and attenuation coefficients are known. A time domain processing technique is used to extract depth and frequency dependent signal ratios for the sample and the reference phantom. The attenuation coefficient and backscatter coefficient of the sample are found from these ratios. The method is tested using tissue-mimicking phantoms with known scattering and attenuation properties.

Key words: Attenuation coefficient; backscatter coefficient; frequency dependence; tissue-mimicking phantom.

I. INTRODUCTION

In medical ultrasound, the backscatter coefficient is commonly used to quantify the scattering properties of a volume of tissue. The backscatter coefficient is defined as the differential scattering cross section per unit volume, measured at a 180° scattering angle. Measurements of backscattering are currently being explored to characterize ultrasonic scattering of excised tissues [1,2] and of tissues in vivo [3,4].

Accurate determinations of the backscatter coefficient must account for instrumental and transmission path factors that affect the scattered signal. To be useful clinically, these determinations also should not be restricted to the far field or the focal region of the transducer. A data reduction method that fulfills the above criteria has been developed by Madsen et al [5], and tested experimentally [6,7]. This method employs a reference specular reflector to compute frequency dependent transmission and reception properties for the transducer-pulser-receiver combination used to record echo signal data. The accuracy of the method may be attributed to the fact that detailed transducer pressure fields are included and the temporal nature of the measurement process is maintained throughout the data reduction.

An important consideration of the above data reduction method is the requirement that precise beam patterns be included in the computations. For

0161-7346/90 $3.00

unfocused or focused single element disk transducers, algorithms have been developed to compute beam patterns based on the geometry of the radiating surface [8]. However, for more complex transducers, such as arrays, computation of the beam pattern is still a major research task. In the present paper, a new method for determining the backscatter coefficient is described. This method requires no explicit knowledge of the transducer beam pattern or the transmission and reception properties of the pulse-echo instrument. It involves comparison of echo data from the sample with data recorded from a reference phantom, whose backscatter coefficient and attenuation coefficient are determined using absolute measurement methods. The reference phantom method has already been suggested by Nicolas [9] and may have advantages because of shorter computation times and the ease with which it could be incorporated into clinical instruments. In this paper we present a detailed derivation of the method as well as results of experimental tests of its accuracy.

II. THEORY

Consider the case in which a transducer, operating in a pulse-echo mode, insonifies a scattering medium and detects the subsequent echoes. The scatterers are assumed to be spatially randomly distributed and the scattered wave fronts spherical in the region of the transducer. Then, the echo signal voltage at time t is given by [5]

$v(t) = \mathrm{Re}\ V(t)$ where

$$V(t) \equiv \int_0^{+\infty} d\omega T(\omega) A_{00}(\omega) e^{-i\omega t}\, \Phi(\omega) \iiint_{\Omega} dr\, N(\mathbf{r}) [A_0(\mathbf{r},\omega)]^2, \qquad (1)$$

and Re means "the real part of" the quantity following. $T(\omega)$ is a complex transfer function relating the net instantaneous force on the transducer at frequency ω to the detected voltage. $A_{00}(\omega)$ is a complex superposition coefficient which, along with the Rayleigh integral, $A_0(\mathbf{r},\omega)$, is used to represent the incident acoustic pulse at point $\mathbf{r}$. $N(\mathbf{r})$ is the number density of scatterers in the neighborhood of $\mathbf{r}$, Φ is the value of the angle distribution factor [10] for the scattered wave, and Ω is the volume containing scatterers in the field. $A_0(\mathbf{r},\omega)$ (see Eq. (4) below) is computed using the size and shape of the piezoelectric element; the function is squared because it also accounts for the scattered wave received at the transducer surface.

When the discrete scatterers are randomly distributed and the scatterer number density is small, only incoherent scattering is important. It can be shown using the methods described in [5] that the ensemble average of $V^*(t)V(t)$ is

$$\overline{V^*(t)V(t)} = \bar{N} \iiint_{\Omega} dr' \int_0^{+\infty} d\omega T^*(\omega) A_{00}{}^*(\omega) e^{i\omega t}\, \Phi^*(\omega) [A_0{}^*(\mathbf{r}',\omega)]^2$$

$$\cdot \int_0^{+\infty} d\omega' T(\omega') A_{00}(\omega') e^{-i\omega' t}\, \Phi(\omega') [A_0(\mathbf{r}',\omega')]^2, \qquad (2)$$

where $N(\mathbf{r})=\bar{N}$, is the average scatterer number per unit volume.

We use a band-pass filter, $P(\omega-\omega_1)$, having a center frequency of ω_1, to filter the echo signal. Call the filtered signal $v(\omega_1,t)$.

$v(\omega_1,t) = \text{Re } V(\omega_1,t)$ where

$$V(\omega_1,t) \equiv \int_0^{+\infty} d\omega T(\omega)A_{00}(\omega)e^{-i\omega t}P(\omega-\omega_1)\Phi(\omega)\iiint_\Omega dr\ N(r)[A_0(r,\omega)]^2.$$

Then

$$\overline{V^*(\omega_1,t)V(\omega_1,t)} =$$

$$\bar{N}\iiint_\Omega dr' \int_0^{+\infty} d\omega T^*(\omega)A_{00}{}^*(\omega)e^{i\omega t}\,\Phi^*(\omega)P(\omega-\omega_1)[A_0{}^*(r',\omega)]^2$$

$$\cdot \int_0^{+\infty} d\omega' T(\omega')A_{00}(\omega')e^{-i\omega' t}\,\Phi(\omega')P(\omega'-\omega_1)[A_0(r',\omega')]^2 \qquad (3)$$

Now, let's take a closer look at the $A_0(r,\omega)$ term.

$$A_0(r,\omega) = \iint_s ds'' \frac{e^{[ik-\alpha(\omega)]|r-r''|}}{|r-r''|} \qquad (4)$$

where the integration is over the surface s of the transducer's active element, r" terminates on area element ds" on s, k is the wavenumber in the propagating medium, and $\alpha(\omega)$ is the attenuation coefficient of the propagating medium. The problem is simplified if the frequency dependent attenuation can be separated from the two-dimensional integral in Eq. (4). If the distance from the transducer to the field point is greater than the diameter of the transducer,

$$A_0(r,\omega) \approx e^{-\alpha(\omega)z}\iint_s ds'' \frac{e^{ik|r-r''|}}{|r-r''|}$$

$$= e^{-\alpha(\omega)z}\,A(r,\omega), \qquad (5)$$

where the origin of the coordinate system is taken to be at the center of the radiating element(s), the z direction being that of the propagating emitted pulses, and $A(r,\omega)$ is $A_0(r,\omega)$ with $\alpha=0$. The position vector of the field point is $r=ix+jy+kz$. A numerical comparison was done for the computation results of $A_0(r,\omega)$ using Eqs. (4) and (5), respectively. The results showed the error caused by this approximation is less for more distal field points and lower frequency transducers. But even at a depth of 2 cm, for a 5.0 MHz 19 mm diameter transducer, the error in computing the ensemble

average voltage squared in Eq. (2) is only 1.8% when the attenuation coefficient is 0.5 db/cm/MHz. Now, Eq. (3) can be rewritten as

$$\overline{V^*(\omega_1,t)V(\omega_1,t)} =$$

$$\bar{N}\iiint_\Omega dr' \int_0^{+\infty} d\omega T^*(\omega)A_{00}{}^*(\omega)e^{i\omega t}\,\Phi^*(\omega)P(\omega-\omega_1)e^{-2\alpha(\omega)z}[A^*(r',\omega)]^2$$

$$\cdot \int_0^{+\infty} d\omega' T(\omega')A_{00}(\omega')e^{-i\omega' t}\,\Phi(\omega')P(\omega'-\omega_1)e^{-2\alpha(\omega')z}[A(r',\omega')]^2. \qquad (6)$$

If the bandwidth of the filter $P(\omega-\omega_1)$ is narrow enough, we can use the values of the scattering function and attenuation at the center frequency for the whole band and remove them from the integral:

$$\overline{V^*(\omega_1,t)V(\omega_1,t)} =$$

$$\bar{N}\Phi^*(\omega_1)\Phi(\omega_1)e^{-4\alpha(\omega_1)z}\iiint_\Omega dr' \int_0^{+\infty} d\omega T^*(\omega)A_{00}{}^*(\omega)e^{i\omega t}\,P(\omega-\omega_1)[A^*(r',\omega)]^2$$

$$\cdot \int_0^{+\infty} d\omega' T(\omega')A_{00}(\omega')e^{-i\omega' t}\,P(\omega'-\omega_1)[A(r',\omega')]^2. \qquad (7)$$

For convenience, we define $I(\omega_1,t)$ and $G(r',\omega_1,t)$ as follows:

$$I(\omega_1,t) \equiv \overline{V^*(\omega_1,t)V(\omega_1,t)} \qquad (8)$$

$$G(r',\omega_1,t) \equiv \int_0^{+\infty} d\omega T(\omega)A_{00}(\omega)e^{-i\omega t}\,P(\omega-\omega_1)[A(r',\omega)]^2. \qquad (9)$$

We have

$$I(\omega_1,t) = BSC(\omega_1)e^{-4\alpha(\omega_1)z}\iiint_\Omega dr'\; G^*(r',\omega_1,t)G(r',\omega_1,t) \qquad (10)$$

where $BSC(\omega_1) = \bar{N}\Phi^*(\omega_1)\Phi(\omega_1)$ is the backscatter coefficient at frequency ω_1.

The significance of Eq. (10) is that we have separated the tissue dependent factors from the instrumentation dependent factors contributing to the mean square scattered signal.

If $BSC(\omega_1)$ and $\alpha(\omega_1)$ are the backscatter coefficient and attenuation coefficient at angular frequency ω_1 for the sample whose properties are to be measured, and $BSC'(\omega_1)$ and $\alpha'(\omega_1)$ are the corresponding values for a reference phantom, then

$$\frac{I(\omega_1,t)}{I'(\omega_1,t)} = \frac{BSC(\omega_1)e^{-4\alpha(\omega_1)z}}{BSC'(\omega_1)e^{-4\alpha'(\omega_1)z}} \equiv \frac{I(\omega_1,z)}{I'(\omega_1,z)} \tag{11}$$

Here, we have mapped the signal at time t to the signal at range z=ct/2, where c is the speed of sound. Also, we have assumed the same speed of sound for both media. (When the speeds are significantly different, a correction is needed.) The ratio of the $I(\omega_1,z)$'s for the unknown sample and the reference phantom at each depth and frequency contains the backscatter coefficient and attenuation coefficient of the sample.

Let $RB(\omega_1)$ be the ratio of the backscatter coefficients of the sample and the reference phantom, and let $\Delta\alpha(\omega_1)$ be the difference in attenuation coefficients of the media. Eq. (11) then becomes

$$\frac{I(\omega_1,z)}{I'(\omega_1,z)} = RB(\omega_1)e^{-4\Delta\alpha(\omega_1)z}. \tag{12}$$

This is the basic equation used to compute the attenuation and backscatter coefficients of the sample.

III. EXPERIMENTAL METHODS

A) Apparatus

Initial tests of this method were done using the setup illustrated in figure 1. The scanner used is an ATL (Advanced Technology Laboratories) Mark III. The sector scanning head has 3 piezoelectric elements mounted on a rotating wheel, 120 degrees apart. Each scan consists of 128 separate pulse-echo sequences, or "acoustic lines." High-voltage impulses excite each transducer. Echo signals received by the transducer are amplified, and then digitized and stored on disk for later analysis.

A LeCroy Model TR8828C high speed transient recorder is used to digitize the RF echo signals. It digitizes +/- 256 mV at 8 bits at a speed of 50 Mega-sample/second in our application. The data are accumulated in the 768 Kbyte memory buffer and then transferred to the MicroVAX via the GPIB interface.

A burst control circuit designed and constructed in our laboratory [11] is used to control the timing. It selects the sector scan lines and the depth range of the rf signal to be digitized. Thus, the control circuit gates on the transient recorder when data from the region of interest are present.

The signal processing for obtaining the filtered amplitude-squared echo data is illustrated in the block diagram in figure 2. $V(\omega_1, t)$, the

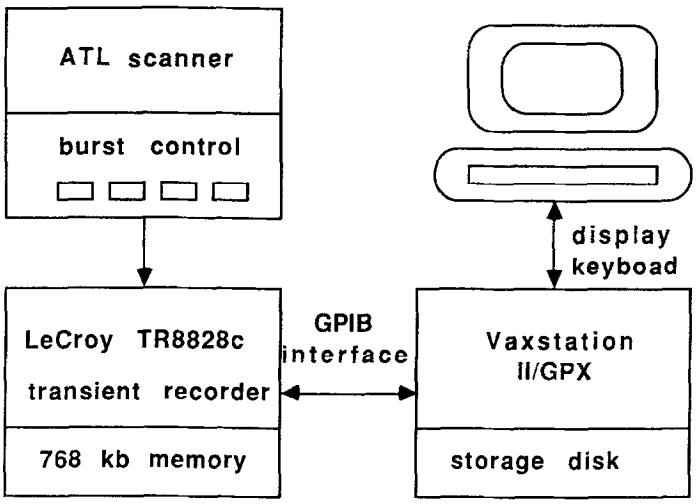

Fig. 1 Setup for digitizing radiofrequency echo signal waveforms from the clinical scanner.

amplitude of the signal at frequency ω_1 and depth z=ct/2, is derived from the echo signal v(t) using

$$V(\omega_1,t) = \int_0^{+\infty} v(t')p(t-t')e^{-i\omega t'}dt'$$

$$= \int_0^{+\infty} v(t')\cos(\omega_1 t')p(t-t')dt' + i\int_0^{+\infty} v(t')\sin(\omega_1 t')p(t-t')dt' \quad (13)$$

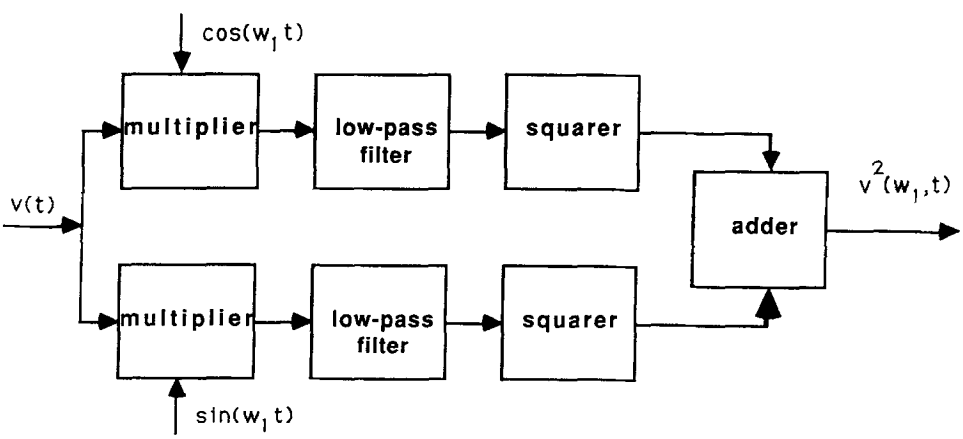

Fig. 2 Flow chart of the time domain signal processing for obtaining amplitude squared data at frequencies of interest from the broadband echo rf waveforms.

where p(t) is a time window. Thus, the echo signal is fed into two channels and multiplied by orthogonal sinusoidal waves with frequency ω_1. p(t-t') is a 3-term Blackman-Harris window [17], which when applied to the signal during the integration serves as a low-pass filter. The voltages output from the low-pass filters are the real and imaginary parts of $V(\omega_1,t)$ weighted by the window area. The length of the time filter window determines the width of the frequency band. A 4 μs window was used in our experiments. The analysis frequency can be flexibly changed by changing the frequency of the reference sinusoidal waves. The method can be easily implemented in hardware, even in analog circuitry. Currently, all processing is done in software using routines written in FORTRAN.

The amplitude squared data are averaged over a number of acoustic lines from a region with similar acoustic properties to form averaged amplitude squared data, $I(\omega_1,z)$, for estimations of acoustic properties.

B. Tissue-like phantoms

Five scattering phantoms were used in the experimental tests of the reference phantom method. Important properties of these phantoms are presented in table 1. The scattering medium in all but one (TM-Liver) consists of microscopic glass spheres randomly distributed in a gel matrix. The backscatter coefficients for these samples can be calculated using the theory of Faran [12] and measured using the absolute method. Phantoms H-4 and B-A also have very finely powdered graphite uniformly distributed throughout the medium, which raises the ultrasonic absorption to that of soft tissues [13]. The graphite particles are small enough that their contribution to the backscatter coefficient is negligible compared to that of the glass beads.

TM-Liver is of different construction than the others. This is a complex phantom with agar spheres surrounded by a matrix material consisting of animal hide gel laced with graphite particles. The agar spheres contain no graphite and have a lower speed of sound and density than the animal hide gel matrix. The diameter of these spheres range from about 0.5 mm to about 2.8 mm with a peak in the distribution at about 1.5 mm [14]. The matrix gel has graphite particles ranging in size from 0.1 to 90 μm. The combination of scatterers has been shown to provide a backscatter coefficient frequency dependence mimicking that of in-vitro liver tissue [15].

Table 1. Properties of the Phantoms used for testing the reference phantom method

Phantom	Attenuation Coefficient α_1 dB/cm/MHz	α_2 dB/cm/MHz^2	Speed of sound m/s	Density g/cm^3	Scatterer Diameter μm
H-2	0.04592	0.0127	1532	1.00	58.8
H-3	0.14050	0.0252	1587	1.02	88.6
H-4	0.44420	0.0198	1580	1.05	88.6
B-A	0.48286	0.0185	1525	1.04	60.5
TM-Liver	0.52900	-0.0020	1540	1.05	-

IV. RESULTS

Initial results were obtained using the H-3 phantom (Table 1) as a reference and H-4 as the "unknown." These phantoms have nearly identical backscatter coefficients but they differ in that phantom H-4 has tissue-like attenuation whereas H-3 has a very low attenuation coefficient. Eighteen scans were taken for the H-3 phantom and 30 for H-4. Fifty adjacent acoustic lines from the center of the image sector were extracted from each scan. Data were recorded from a depth range of 1-5 cm in both phantoms.

Figure 3 presents the $I(\omega,z)/I'(\omega,z)$ results (Eq. (12)) at 2.5 MHz, 4 MHz and 5.5 MHz for these two phantoms. Variations in the curves for each frequency are a result of statistical fluctuations in the data. These curves are free of instrumental factors, depending only on the properties of the phantoms. The decline of the ratios with depth in figure 3 is due to the difference between the attenuation coefficients of the two phantoms.

The attenuation coefficient at frequency ω of the unknown sample, $\alpha(\omega)$ is determined by computing the logarithm of the corresponding ratio at each depth and fitting these data to a straight line. The slope of the line is $4[\alpha(\omega)-\alpha'(\omega)]$ where $\alpha'(\omega)$ is the attenuation coefficient of the reference phantom. Table 2 presents the attenuation coefficient of the H-4 phantom at several frequencies, obtained using this method. Also shown are attenuation results obtained using a narrow band substitution technique [13] applied to a test cylinder constructed when the H-4 phantom was formed. Results are in agreement to within 4% at 2.5 MHz, and closer agreement is seen at higher frequencies.

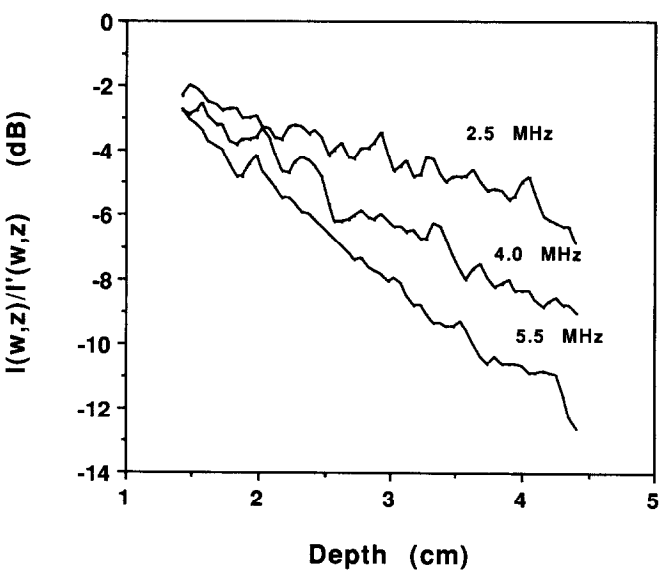

Fig. 3 The ratio of the average amplitude-squared for phantoms H-4 and H-3. The decline of the ratios with depth is due to the difference between the attenuation coefficients of the two phantoms.

Table 2. Attenuation coefficients of phantom H-4 obtained using the reference phantom method (RPM), compared with results of a narrow band substitution method

Frequency (MHz)	RPM (S.D.) (dB/cm)	Substitution method (dB/cm)
2.5	1.18 (0.12)	1.23
3.0	1.47 (0.13)	1.51
3.5	1.78 (0.14)	1.79
4.0	2.10 (0.14)	2.09
4.5	2.42 (0.16)	2.40
5.0	2.76 (0.16)	2.72
5.5	3.12 (0.17)	3.04

S.D. is the standard deviation caused by statistical fluctuations.

Table 3 presents results for the ratio of the backscatter coefficients RB(ω). In this example, the two phantoms have nearly identical backscatter coefficients, so the RB(ω)'s should approach 0 dB. The largest deviation occurred at 5 MHz and corresponds to an error of 36%, with significantly smaller errors at other frequencies.

Figures 4 and 5 show attenuation and backscatter coefficients for the B-A phantom, where the H-2 phantom was used as a reference. Three different transducers with center frequencies of 2.25, 3.5 and 5.0 MHz were used to extend the measurement over the range shown. Sixty-four statistically independent acoustic lines were used to compute I(ω,z) data and then give a measurement of both the attenuation coefficient and the backscatter coefficient. The error bars represent ±1 standard deviation for 10 such measurements.

Table 3. The ratio of the backscatter coefficient in the H-4 phantom to that in the H-3 phantom, using the reference phantom method. The ratio (RB(ω)) is expressed in decibels and is presented for 7 frequencies

Frequency (MHz)	RB(ω) (dB)
2.5	0.03
3.0	-0.02
3.5	0.26
4.0	0.53
4.5	0.72
5.0	1.35
5.5	0.77

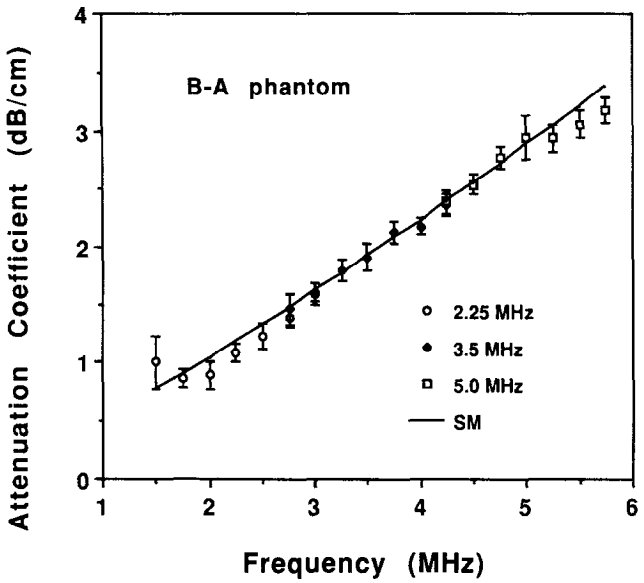

Fig. 4 Attenuation coefficients of phantom B-A measured using three transducers to cover a wide frequency range. The data points are from the reference phantom method while the solid line is a result of curve fitting the data from the narrow band substitution method.

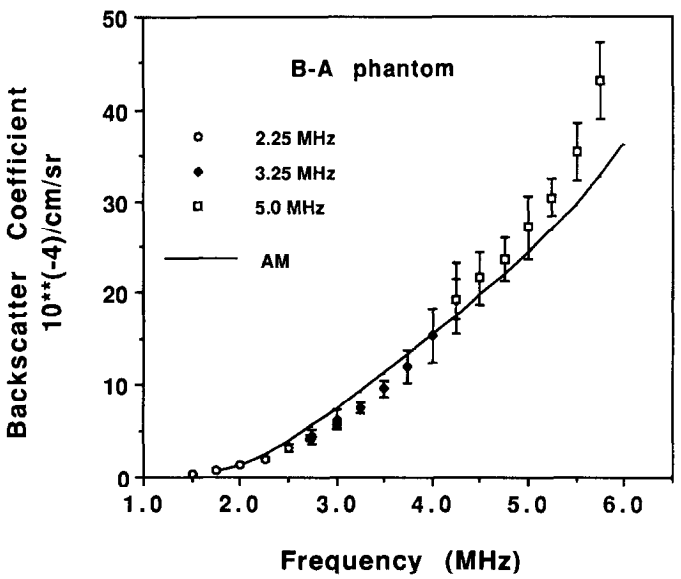

Fig. 5 Backscatter coefficients of phantom B-A. The data points are from the reference phantom method and the solid line is a result of curve fitting the data from the absolute method.

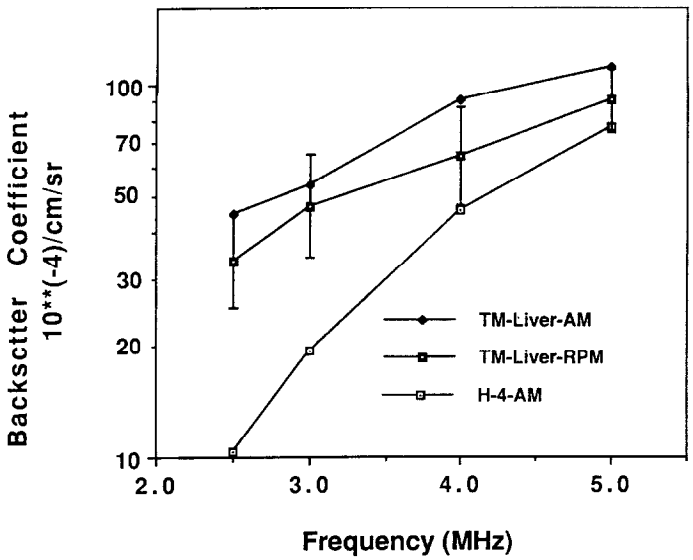

Fig. 6 Backscatter coefficient of TM-Liver vs. frequency. Closed data points were obtained using the absolute method while the open squares are data from the reference phantom method. Also shown is the backscatter coefficient of the Rayleigh scattering phantom H-4 used as a reference.

The continuous curve is calculated using $\alpha(f) = (0.48286\ f + 0.0185\ f^2)$ dB/cm in figure 4, where f is the frequency in MHz (see table 1). These parameters were obtained by curve fitting the attenuation data from narrow band substitution measurements [13] applied to test cylinders containing the same material as in the B-A phantom. Results obtained with the reference phantom method are shown by data points.

In figure 5, the solid curve is the result of curve fitting backscatter coefficients measured using the absolute method [5]; the data points are results of measurements using the reference phantom. Except for the 28% error at higher frequencies, the reference phantom method did quite well in yielding the backscatter coefficient.

The H-4 phantom was used as a reference to measure the backscatter coefficients of TM-Liver. The results are shown in figure 6. Also shown are the results from the absolute method for both TM-Liver and the H-4 phantom. The frequency dependence of the backscatter coefficients of TM-Liver is quite different from that of H-4 Rayleigh scattering phantom. In spite of this, the reference phantom method appears to yield satisfactory results for the backscatter coefficient in this material.

IV. DISCUSSION AND CONCLUSIONS

The reference phantom method, as described and implemented in this paper, appears to work well for determining the frequency dependent attenuation and

backscatter coefficient in volumes where these parameters can be considered uniform. The method yielded results that are in agreement with those obtained using an absolute data reduction method, even when the frequency dependence of scattering in the sample was different from that of the reference phantom. This finding has important clinical implications since the TM-liver phantom used in this study has a frequency dependence of scattering that mimics scattering from human liver.

Hall [16] has determined that errors of 100% or higher in the backscatter coefficient can occur if the frequency dependence of scatter is not included in the data analysis for broadbanded pulses and short time gates. In the present work, this effect is minimized using a relatively long duration (4 μs) analysis window convolved with the echo data. If shorter windows are used, this could lead to significant errors in determining the backscatter coefficient when the scattering and/or attenuation properties of the reference phantom differ significantly from those of the sample measured.

An advantage of the reference phantom method over our previous method of data analysis [5] is that since no pressure field computations are used, it may be more easily incorporated into clinical instruments, including those with rectangular arrays. Also, since the signal processing is done in the time domain, it can be implemented easily either in software or hardware, and could be done in real time.

Finally, it is important to keep in mind that the accuracy of this method depends on the accuracy to which the attenuation and backscatter coefficients of the reference phantom are known at the analysis frequencies. Thus, phantoms used in this application must be provided with accurate calibrations by absolute measurement methods.

ACKNOWLEDGMENTS

This work was supported by Grants RO1-CA25634 and RO1-CA39224 from the National Institutes of Health. We are grateful to Dr. Evan Boote for constructing the burst control circuit and developing the algorithms for data acquisition.

REFERENCES

[1] Fei, D.Y. and Shung, K.K., Ultrasonic backscatter from mammalian tissues, J. Acoust. Soc. Am. 78, 871-876 (1985).

[2] D'Astous, F. and Foster, F., Frequency dependence of ultrasound attenuation and backscatter in breast tissue," Ultrasound Med. Biol. 12, 795-808 (1986).

[3] Lizzi, F.L., King, D.L., Rorke, M.C., Hui, J., Ostromogilsky, M., Yaremko, M.M., Feleppa, E.J. and Wei, P., Comparison of theoretical scattering results and ultrasonic data from clinical liver examinations, Ultrasound Med. Biol. 14, 377-385, (1988).

[4] Garra, B.S., Insana, M.F., Shawker, T.H., Wagner, R.F., Bradford, M., and Russell, M., Quantitative ultrasonic detection and classification of diffuse liver disease comparison with human observer performance, Investigative Radiology 24, 196-203, (1989).

[5] Madsen, E.L., Insana, M.F., Zagzebski, J.A., Method of data reduction for accurate determination of acoustic backscatter coefficients, J. Acoust. Soc. Am 76, 913-923 (1984).

[6] Insana, M.F., Madsen, E.L., Hall, T.J., and Zagzebski, J.A., Tests of the accuracy of a data reduction method for determination of acoustic backscatter coefficients, J. Acoust. Soc. Am. 79, 1230-1236 (1986).

[7] Hall, T.J., Madsen, E.L., Zagzebski, J.A., and Boote, E.J., Accurate depth-independent determination of acoustic backscatter coefficients with focused transducers, J. Acoust. Soc. Am. 85, 2410-2416, (1989).

[8] Madsen, E.L., Goodsitt, M.M., and Zagzebski, J.A., Continuous waves generated by focused radiators, J. Acoust. Soc. Am. 70, 1508-1517 (1981).

[9] Nicolas, J., A New Method for the Analysis of the Frequency Dependence of the Backscattering Coefficient in Tissue-like Media, in Acoustical Imaging, Vol. 14, A. Berkhout, J. Ridder and L. Van der Wal, eds., pp. 761-764 (Plenum Press, New York, 1985).

[10] Morse, P.M., and Ingard, K.U., Theoretical Acoustics, p. 411, (McGraw-Hill, New York, 1968).

[11] Boote, E.J., Zagzebski, J.A., Madsen, E.L., and Hall, T.J., Instrument independent acoustic backscatter coefficient imaging, Ultrasonic Imaging 10, 121-138 (1988).

[12] Faran, J.J., Sound scattering by cylinders and spheres, J. Acoust. Soc. Am. 23, 405-418 (1951).

[13] Madsen, E.L., Zagzebski, J.A., Banjavic, R., and Jutila, R., Tissue-mimicking materials for ultrasound phantoms, Med. Phys. 5, 391-394 (1978).

[14] Insana, M.F., Methods for Measuring Ultrasonic Backscatter and Attenuation Coefficients for Tissues and Tissue-like Media, Ph.D. Thesis, University of Wisconsin, Madison, 1983.

[15] Madsen, E.L., Zagzebski, J.A., Insana, T.M., Burke, T.M., and Frank, G., Ultrasonically tissue-mimicking liver including the frequency dependence of backscatter, Med. Phys. 9, 703-709 (1982).

[16] Hall, T.J., Experimental Methods for Accurate Determination of Acoustic Backscatter Coefficients, Ph.D. Thesis, University of Wisconsin, Madison, 1988.

[17] Harris, F.J., On the use of windows for harmonic analysis with the discrete Fourier transform, Proceedings IEEE 66, 51-83 (1978).